Applied Science and Innovative Research
ISSN 2474-4972 (Print) ISSN 2474-4980 (Online)
Vol. 10, No. 1, 2026
www.scholink.org/ojs/index.php/asir

Original Paper

Modeling Spatial Distribution of Humidity and Near-surface Soil Temperature in Common Greenhouses

Zhenyu Li[1], Xin Meng[1*], Renhe Zhai[1], Shaojie Wang[1], Dong Wang[1] & Jiang Li[2]

[1] School of Mechanical Engineering, Shaanxi University of Technology, Hanzhong 723001, China

[2] Hanzhong Yifeng Huamao Agricultural Technology Development Co., Ltd., China

[*] Corresponding Author: Xin Meng

Received: January 16, 2026 Accepted: March 2, 2026 Online Published: March 9, 2026

doi:10.22158/asir.v10n1p94 URL: http://dx.doi.org/10.22158/asir.v10n1p94

Abstract

To overcome the limited adaptability of current greenhouse environmental models, this study develops targeted models for predicting the spatial distribution of near-surface soil temperature and air humidity. The soil temperature model utilizes a one-dimensional unsteady-state heat transfer approach that accounts for solar radiation, convection, thermal radiation, and evaporation. Concurrently, the air humidity model applies water vapor mass conservation to integrate the effects of soil evaporation, ventilation, and humidification.

Experimental validation showed that the soil temperature model effectively captured diurnal variations at different soil depths. The relative root mean square error (rRMSE) was 5% at 0.25 m depth, demonstrating high accuracy, whereas predictions at the more dynamic surface layer (0.05 m) showed a higher error of 10%. The air humidity model produced trends consistent with measured data, albeit with a general underestimation, yielding a mean bias error (MBE) of 4.027 and an RMSE of 8.09%.

The proposed models exhibit strong adaptability for simulating humidity and near-surface soil temperature distributions in common greenhouses. This work provides valuable insights and a practical methodological framework for advancing precise environmental control and promoting the development of standardized models in facility agriculture.

Keywords

Greenhouse, Near-surface Soil, Temperature Distribution, Air humidity

Nomenclature

t: soil temperature, ℃	Δ: slop of saturation line on psychrometric chart, kPa/K
τ: time, h	Pa: vapor pressure of ambient air, kPa
a: thermal diffusivity, m²/s	Γ: psychrometric constant, kPa/K
x: the depth of soil, m	t_0: outdoor air temperature, ℃
λ: thermal conductivity of soil, W/(℃·m)	ε_s: system emissivity
q_c: the convection heat transfer between the soil surface and indoor air, W/m²	ε_1: emissivity of soil
q_s: the solar radiation absorbed by the ground, W/m²	ε_2: emissivity of the film plane
q_e: soil water evaporation, W/m²	A_1: soil area, m²
q_r: thermal radiation loss of soil, W/m²	A_2: the film plane area, m²
h_c: convective heat transfer coefficient, W/(℃·m)	σ: Stefan-Boltzmann constant
t_f: indoor air temperature,℃	T_f: daily mean Kelvin temperature of indoor air, K
α: solar absorptivity of soil	T_2: Kelvin temperature of the film plane, K
h_r: radiation heat transfer coefficient, W/(℃·m)	A_n: amplitude of solar-air temperature
φ_n: delay of solar-air temperature	ω: frequency of solar-air temperature
n: the order of simple harmonic wave of solar-air temperature	

Introduction

In the global context of agricultural modernization, greenhouses serve as essential components of facility agriculture. They have transcended the seasonal and regional constraints inherent in traditional agricultural production by actively regulating environmental factors such as light, temperature, and humidity. This regulation provides stable and controllable growth environments for high-value crops, including morel mushrooms. Since the introduction of the glass greenhouse prototype in the 19th century, greenhouse technology has progressively evolved from passive collection of light and heat to intelligent and precise environmental control. Among various types of greenhouses, solar greenhouses are notable for their thick walls and multi-layer covering systems that efficiently accumulate solar energy. These structures are equipped with ventilation and shading devices, making them particularly suitable for large-scale production requiring significant investment. In contrast, ordinary greenhouse sheds—characterized by light steel frameworks or bamboo and wood constructions covered with single-layer plastic films—have become the predominant choice among rural areas and small to medium-sized farmers in China due to their simple structure, flexible construction options, and low cost. Statistical data indicate a steady increase in the number of greenhouses across China; currently, this country holds first place globally in terms of greenhouse numbers. As of 2022, the total area dedicated to greenhouses reached approximately 1.862 million hectares. The "National Modern Facility Agriculture Construction Plan (2023-2030)" explicitly emphasizes: "We should focus on developing energy-saving solar greenhouses and greenhouse sheds while promoting new materials and innovative shed designs to enhance winter warmth retention

capabilities as well as summer heat dissipation." This statement underscores both the urgency for intelligent upgrades within small- to medium-sized greenhouse sheds and a clear policy direction moving forward.

At present, scholars both domestically and internationally have conducted extensive research on the construction and control technologies of greenhouse environment models, thereby laying a solid foundation for the intelligent development of facility agriculture. In the realm of model construction, Sun Yabo et al. [3] established a dynamic simulation model to analyze temperature and humidity in photovoltaic solar greenhouses. Their work elucidated the influence of various photovoltaic installation methods (including upper half laying, checkerboard laying, and full laying) on indoor environmental conditions, providing theoretical support for the design and temperature-humidity control within photovoltaic greenhouses. Deng et al. [4] developed an analytical model addressing surface temperature and thermal balance in bare soil within solar greenhouses by integrating factors such as soil moisture evaporation, solar radiation, thermal radiation, and convective heat transfer. Their findings indicated that during daylight hours, solar radiation serves as the primary source of energy for soil; conversely, heat loss predominantly occurs through water evaporation during this time while at night it is primarily due to thermal radiation. Furthermore, Chen Jinxuan et al. [5], utilizing principles from heat and mass transfer theory alongside an analysis of heat balance in enclosure structures relative to air moisture balance, constructed a predictive model for indoor temperature and humidity in solar greenhouses. The relative errors between their predictions and two-day measured data were found to be as low as 5.11% and 4.17%, respectively—demonstrating high prediction accuracy. In terms of optimizing prediction methodologies, Pan Jigang et al. [6] employed Spearman correlation analysis to select key environmental factors before enhancing the Elman neural network with a sparrow search algorithm. This approach successfully reduced the mean square error for temperature predictions to 0.592 with an average error of 0.320; similarly achieving a mean square error for humidity predictions at 0.120 with an average error of 2.530. Feng Daguang et al. [7] integrated cluster analysis, time series analysis, and multiple linear regression models to optimize the temperature prediction model using the sum of squared errors as the evaluation criterion. This approach enhanced prediction stability in complex environments. In tropical and humid conditions, Vita et al. [8] determined the component heat exchange constant by analyzing temperature variations both inside and outside the greenhouse. The mean square error of their established model was merely 0.0085, while the model efficiency (Ef) reached an impressive 0.99, indicating exceptional environmental adaptability.

At the level of control framework innovation, Kim et al. [9] proposed a Gaussian process-based stochastic model predictive control (GP-SMPC) framework that probabilistically captures the uncertainties arising from variations in crop growth and fluctuations in outdoor weather conditions. Compared to traditional nonlinear model predictive control (MPC), tracking errors were reduced by 67% and 48% during winter and spring, respectively, while energy and CO_2 costs decreased by 51.4% and 40%, respectively. Xiong et al. [10] introduced a hybrid modeling approach that integrates a mechanistic model with long short-

term memory (LSTM) neural networks, significantly enhancing prediction accuracy in complex environments by correcting uncertain climate data through neural network residuals. Mahmood et al. [11] designed an improved model predictive control framework wherein the primary controller provided the nominal trajectory while the auxiliary controller adjusted for uncertainties; average absolute errors recorded in winter and summer were merely 0.09°C and 0.10°C, respectively, with root mean square errors of 0.19°C and 0.36°C, respectively. Mallick et al. [12] validated the effectiveness of fuzzy logic controllers (FLC) within climate automation systems for smart insulated greenhouses (SIG), achieving root mean square errors for temperature and humidity predictions of just 0.69% and 0.23%, respectively, alongside control efficiency factors reaching as high as 99.35% and 99.86%. Bernardo et al. [13] incorporated deep deterministic policy gradient (DDPG) techniques from reinforcement learning (RL) to compare performance differences between model predictive control (MPC) and RL within a unified framework, thereby providing new avenues for controlling large continuous state-action spaces in greenhouse environments Oybek et al. [14] assessed the performance of deep neural networks, Long Short-Term Memory (LSTM) networks, and one-dimensional convolutional neural networks in climate prediction for hydroponic greenhouses. Their findings indicated that the LSTM model exhibited a significant advantage in short-term interval predictions. Akshay et al. [15] proposed an AI-driven semi-closed greenhouse control framework and conducted a comparative analysis of deterministic equivalent Model Predictive Control (MPC), robust MPC, and deep deterministic policy gradient methods. The results demonstrated that energy consumption was reduced by 57% compared to traditional control approaches, while the deviation from the set value improved by over 26.8% relative to the baseline method.

Although a substantial body of research exists, three critical areas have received relatively little attention regarding the commonly utilized ordinary greenhouse in China. First, there is a misalignment in research subjects. The prevailing models predominantly focus on high-cost multi-span intelligent greenhouses or photovoltaic solar greenhouses [3-8, 9-15], neglecting the fundamental structural characteristics of ordinary greenhouses (light steel structure and single-layer film covering). This oversight results in poor model adaptability and challenges in direct application. Second, core processes are often overlooked. Existing soil temperature models [4, 7] typically do not address the unique heat transfer characteristics of near-surface soil within greenhouses (0.05 - 0.25m), which is crucial for crop root development. Furthermore, these models fail to systematically incorporate dynamic factors such as solar radiation and soil moisture evaporation, leading to inadequate accuracy in predicting shallow soil temperatures. Third, there exists an imbalance between cost and precision. Most intelligent models depend on complex sensor networks and high-performance computing equipment [5-6, 9-12], without taking into account the financial constraints faced by small and medium-sized farmers. Consequently, they fall short of addressing the practical demand for "low-cost intelligence." Therefore, This study presents a simplified yet comprehensive model that integrates key heat and mass transfer processes for practical application in resource-constrained greenhouse environments. Using a common greenhouse designed for cultivating

morel mushrooms in Hanzhong, Shaanxi Province as the experimental subject, the accuracy of the models is validated through measured data of soil temperature at various depths and air humidity levels. The objective is to provide a theoretical framework and technical solution that are both economical and precise for the low-cost intelligent transformation of small- to medium-sized greenhouse structures.

Materials and methods

Analysis of Greenhouse Soil Heat Conduction

The greenhouses investigated in this study exhibit light steel structures as frameworks and single-layer plastic film covering. Unlike the complex and costly structures of multi-span intelligent greenhouses, they are characterized by simple flexibility and low construction costs. The analysis of soil heat conduction within greenhouses is outlined in Figure 1. The heat transfer process primarily incorporates solar radiation, soil evaporation, long-wave thermal radiation, convective heat transfer, and soil heat conduction. Energy is derived from solar radiation, wherein soils gain heat through solar radiation and lose heat via water evaporation, while both thermal radiation and convective heat transfer simultaneously occur between the soil and air. During soil heat transfer, solar radiation, q_s, represents the energy absorbed by the soil (positive value), while convective heat transfer, q_c, is the convective heat exchange between the greenhouse air and soil (positive value). In addition, soil radiation, q_r, is the heat lost through radiative heat transfer between the soil and plastic film (negative value), while q_e is the heat lost during soil water evaporation (negative value).

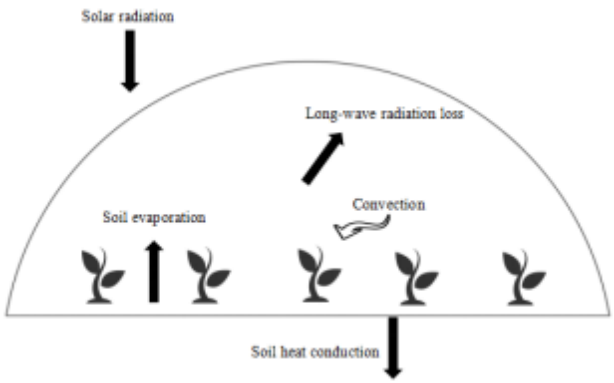

Figure 1. Schematic Showing the Analysis of Soil Heat Conduction in Greenhouses

Greenhouse Temperature Prediction Model

The following assumptions are made for greenhouse soil heat transfer processes.

1.Heat transfer in greenhouse soils is one-dimensional.

2.Greenhouse soil is regularly irrigated soil moisture is sufficient.

3.The temperature and solar radiation in greenhouses follow a 24-hour cycle, and the boundary conditions of the soil periodically change.

Based on the above assumptions, the heat transfer model for greenhouse soils can be expressed by the following formula:

$$\begin{cases} \dfrac{\partial t}{\partial \tau} = a\dfrac{\partial^2 t}{\partial x^2} \\ x = 0, -\lambda\dfrac{\partial t}{\partial x} = q_c + q_s - q_e - q_r \end{cases} \tag{1}$$

where t is the soil temperature, τ is the time, a is the thermal diffusivity of the soil, x is soil depth, λ is soil thermal conductivity, q_c is the convective heat transfer between the soil surface and the greenhouse air, q_s is the solar radiation absorbed by the ground, q_e is soil water evaporation, and q_r is the thermal radiation loss from the soil.

To fully account for the influence of different boundary conditions, such as water evaporation and solar radiation, on the soil surface, solar-air temperature is introduced to simplify the equation and can be expressed as:

$$x = 0, -\lambda\frac{\partial t}{\partial x} = h\left(t_{\text{solar}-\text{air}} - t\right) \tag{2}$$

When soil boundary conditions periodically change, the solar-air temperature can be expressed as:

$$t_{\text{solar}-\text{air}} = \bar{t}_{\text{solar}-\text{air}} + \sum_{i=1}^{\infty} A_n \cdot \sin\left(n\omega\tau + \varphi_n\right) \tag{3}$$

where $\bar{t}_{\text{solar-air}}$ is the daily average, n is the order of the simple harmonic wave, ω is the frequency, An is the amplitude, and φ_n is the phase delay of the solar-air temperature.

For the periodic heat transfer in a semi-infinite soil (Zhang, 2014) [16], the expression for the soil temperature distribution is:

$$t(x,\tau) = \bar{t}_{\text{solar}-\text{air}} + \sum_{i=1}^{\infty} \phi_n A_n \exp\left(-x\sqrt{\frac{n\omega}{2a}}\right) \cdot \sin\left(n\omega\tau + \varphi_n - x\sqrt{\frac{n\omega}{2a}} - \psi_n\right) \tag{4a}$$

$$\phi_n = \frac{1}{\sqrt{1 + 2\dfrac{\lambda}{h}\sqrt{\dfrac{n\omega}{2a}} + 2\dfrac{\lambda^2}{h^2}\dfrac{n\omega}{2a}}} \tag{4b}$$

$$\psi_n = \arctan\left(\frac{1}{1 + \dfrac{h}{\lambda}\sqrt{\dfrac{2a}{n\omega}}}\right) \tag{4c}$$

In solar greenhouses, soils have special boundary conditions. Therefore, calculation of the solar-air temperature is critical for soil temperature calculation in solar greenhouses. Tiwari, G. N. [17] proposed an equation for calculating the solar-air temperature of moist surfaces, but fails to consider the unique heat transfer mechanisms of greenhouses, making it difficult to directly apply to solar greenhouses.

Consequently, combining the heat transfer conditions of the soil surface in solar greenhouses is necessary to derive an equation for calculating the solar-air temperature of soil surfaces in solar greenhouses.

The convective heat transfer between the soil and the greenhouse interior air can thus be expressed as:

$$q_c = h_c\left(t_{\mathrm{f}} - t\right) \tag{5}$$

where, qc represents the convective heat transfer between the soil surface and indoor air, hc is the convective heat transfer coefficient, and tf is the indoor air temperature.

In the absence of artificial ventilation, the flow regime at the soil surface of solar greenhouses is natural convection turbulence. Consequently, the convective heat transfer coefficient can be calculated with the formula:

$$h_c = 1.52 \cdot \left(\Delta \mathrm{T}\right)^{1/3} \tag{6}$$

where ΔT is the temperature difference between the soil and air inside the solar greenhouse.

The solar radiation absorbed by the ground is related to the solar absorptivity of the soil and reflectivity of the film. The solar radiation absorbed by the ground can be expressed as [18]:

$$q_s = \alpha \cdot A \cdot R_{\mathrm{s}} \cdot \left(1 - \mathrm{r_{cs}}\right) \cdot \mathrm{e}^{-\mathrm{k \cdot LAI}} \tag{7}$$

where qs is the solar radiation absorbed by the ground, α is the solar absorptivity of the soil, A is the surface area of the greenhouse covering material, Rs is the solar radiation, and rcs is the reflectivity of the film.

Soil water evaporation is related to solar radiation, soil water content, and air relative humidity. The amount of soil water evaporation can therefore be expressed as [17]:

$$q_e = \frac{\Delta \cdot q_s + h_c \cdot \mathrm{Pa}\left(1 - \mathrm{Y}\right)}{\Gamma + \Delta} \tag{8}$$

where q_e is the soil water evaporation amount, Δ is the slope of the saturation line on the psychrometric chart, q_s is the solar radiation absorbed by the ground, h_c is the convective heat transfer coefficient, Pa is the vapor pressure of ambient air, Y is the relative humidity of indoor air, and Γ is the psychrometric constant.

The radiative heat transfer between the greenhouse soil and the film can then be expressed as [16]:

$$\mathrm{q_r} = \mathrm{h_r}\left(t - \mathrm{t_f}\right) + \varepsilon_{\mathrm{s}} \cdot \sigma\left(\mathrm{T_f^4} - \mathrm{T_2^4}\right) \tag{9}$$

where q_r is the thermal radiation loss from the soil, and ε_s is the system emissivity that is related to ε_1 (soil emissivity), ε_2 (film emissivity), A_1 (soil area), A_2 (film planar area), and $X_{1,2}$ (the radiation view factor from the soil to the film plane). ε_s can be calculated as $\varepsilon_{\mathrm{s}} = \frac{1}{\frac{1-\varepsilon_1}{\varepsilon_1} + \frac{1}{\mathrm{X_{1,2}}} + \frac{1-\varepsilon_2}{\varepsilon_2} \cdot \frac{\mathrm{A_1}}{\mathrm{A_2}}}$, wherein σ is the Stefan-Boltzmann constant, T_f is the daily average Kelvin temperature of the indoor air, T_2 is the Kelvin

temperature of the film, and h_r is the radiative heat transfer coefficient that can be expressed as: $\mathrm{h_r} = 4\varepsilon_s \cdot \sigma\left(\overline{\mathrm{T}}_\mathrm{f}\right)^3$.

The analysis of convective heat transfer between soil and air in the sunlight greenhouse, solar radiation absorbed by the soil, soil moisture evaporation, and thermal radiation loss of the soil can allow calculation of the boundary condition at the soil surface (x = 0) via the following equation:

$$-\lambda\frac{\partial \mathrm{t}}{\partial \mathrm{x}} = h_c\left(t_f - t\right) + \alpha\cdot\mathrm{A}\cdot R_\mathrm{s}\cdot\left(1-\mathrm{r_{cs}}\right)\cdot\mathrm{e}^{-\mathrm{k}\cdot LAI} - \frac{\Delta\cdot q_s + \mathrm{h}\cdot\mathrm{P_a}\left(1-\mathrm{Y}\right)}{\Gamma+\Delta} - h_r\left(t-\mathrm{t_f}\right) - \varepsilon_\mathrm{s}\sigma\left(\mathrm{T_f^4} - \mathrm{T_2^4}\right) \tag{10}$$

Formula (2) can also be rewritten as:

$$-\lambda\frac{\partial t}{\partial x} = \left(h_r + h_c\right)\left(t_{\mathrm{solar-air}} - t\right) \tag{11}$$

By combining Formulas (10) and (11), the expression for the solar-air temperature of the soil in the greenhouse can be derived via the following equation:

$$t_{\mathrm{solar-air}} = t_f + \left(\frac{1}{h_r+h_c} - \frac{1}{h_r+h_c}\cdot\frac{\Delta}{\Gamma+\Delta}\right)\alpha\cdot\mathrm{A}\cdot R_\mathrm{s}\cdot\left(1-\mathrm{r_{cs}}\right)\cdot\mathrm{e}^{-\mathrm{k}\cdot LAI} - \frac{h_c}{h_r+h_c}\cdot\frac{\mathrm{Pa}\cdot\left(1-\mathrm{Y}\right)}{\Gamma+\Delta} - \frac{1}{h_r+h_c}\varepsilon_\mathrm{s}\sigma\left(\mathrm{T_f^4} - \mathrm{T_2^4}\right) \tag{12}$$

Consequently, the overall equation for solving the near-surface soil temperature distribution in greenhouses is as follows:

$$\begin{cases} t_{\mathrm{solar-air}} = t_f + \left(\dfrac{1}{h_r+h_c} - \dfrac{1}{h_r+h_c}\cdot\dfrac{\Delta}{\Gamma+\Delta}\right)\alpha\cdot\mathrm{A}\cdot R_\mathrm{s}\cdot\left(1-\mathrm{r_{cs}}\right)\cdot\mathrm{e}^{-\mathrm{k}\cdot LAI} - \dfrac{h_c}{h_r+h_c}\cdot\dfrac{\mathrm{Pa}\cdot\left(1-\gamma\right)}{\Gamma+\Delta} - \dfrac{1}{h_r+h_c}\varepsilon_\mathrm{s}\sigma\left(\mathrm{T_f^4} - \mathrm{T_2^4}\right) \\ t_{\mathrm{solar-air}} = \bar{t}_{\mathrm{solar-air}} + \sum_{i=1}^{\infty}\mathrm{A}_n\cdot\sin\left(n\omega\tau + \varphi_n\right) \\ t\left(x,\tau\right) = \bar{t}_{solar-air} + \sum_{i=1}^{\infty}\phi_n\mathrm{A}_n\exp\left(-x\sqrt{\dfrac{n\omega}{2a}}\right)\cdot\sin\left(n\omega\tau + \varphi_n - x\sqrt{\dfrac{n\omega}{2a}} - \psi_n\right) \\ \phi_n = \dfrac{1}{\sqrt{1+2\dfrac{\lambda}{\left(h_r+h_c\right)}\sqrt{\dfrac{n\omega}{2a}} + 2\dfrac{\lambda^2}{\left(h_r+h_c\right)^2}\dfrac{n\omega}{2a}}} \\ \psi_n = \arctan\left(\dfrac{1}{1+\dfrac{\left(h_r+h_c\right)}{\lambda}\sqrt{\dfrac{2a}{n\omega}}}\right) \end{cases} \tag{13}$$

This expression combines radiative, convective, and evaporative fluxes into an effective boundary condition.

Greenhouse Humidity Prediction Model

Based on the law of conservation of mass and taking into account the water vapor balance processes within the greenhouse—such as soil evaporation, humidification, and ventilation—the net water vapor input can be expressed as the sum of soil evaporation ($\mathrm{E_{soil}}$) and humidification (Mhumid[t]), minus the water vapor removed by ventilation $V_{\mathrm{vent}}\cdot\dfrac{RH_{\mathrm{in}}\left[\mathrm{t}\right] - RH_{\mathrm{out}}}{100}\cdot\rho_{\mathrm{sat}}$. The maximum total amount of water

vapor that the air inside the greenhouse can accommodate is given by $V_{air} \cdot \rho_{sat}$. Furthermore, to convert relative humidity differences into absolute quantities of water vapor, one must divide by 100. Consequently, we derive the formula for the rate of change in indoor humidity within the greenhouse as follows:

$$\frac{\mathrm{d}RH_{\mathrm{in}}}{\mathrm{d}t} = \frac{E_{soil} + M_{\mathrm{humid}}[t] - V_{\mathrm{vent}} \times \frac{RH_{\mathrm{in}}[t] - RH_{\mathrm{out}} \times \rho_{\mathrm{sat}}}{100}}{\mathrm{V}_{\mathrm{air}} \times \rho_{\mathrm{sat}}} \tag{14}$$

where E_{soil} is the soil evaporation amount, Mhumid[t] is the humidification amount at time t (unit: g/h), RH_{out} is the outdoor humidity (unit: %), V_{air} is the indoor air volume, ρ_{sat} is the saturated water vapor density, and V_{ent} is the ventilation rate.

The saturated water vapor density represents the maximum capacity of water vapor that can be contained in the air at a given temperature. This relationship is expressed by the Magnus formula in terms of the indoor temperature, T_{in} (unit: °C), as follows:

$$\rho_{\mathrm{sat}} = 216.7 \times \mathrm{e}^{\frac{17.67 \times T_{\mathrm{in}}}{T_{\mathrm{in}} + 243.5}} \tag{15}$$

The soil evaporation level is related to differences between the current indoor humidity, $RH_{in}[t]$ (unit: %), and the set reference humidity of 90%, as determined by the soil evaporation coefficient k_{soil} (unit: g/(h·%)). Soil evaporation can be calculated with the following equation:

$$E_{\mathrm{soil}} = \mathrm{k}_{\mathrm{soil}} \times (90 - RH_{\mathrm{in}}[t]) \tag{16}$$

The ventilation rate is affected by the basic ventilation rate V_{base} (unit: m^3/h) and the temperature difference between indoor and outdoor, as calculated with the following equation:

$$V_{\mathrm{vent}} = V_{\mathrm{base}} + 20 \times (T_{\mathrm{in}} - T_{\mathrm{out}}) \tag{17}$$

where T_{out} is the outdoor temperature (unit: °C).

The updated formula for indoor humidity leverages Euler's method to recursively update humidity over time, is expressed as:

$$RH_{\mathrm{in}}[t+1] = RH_{\mathrm{in}}[t] + \frac{dRH_{in}}{dt} \times \frac{\Delta t}{60} \tag{18}$$

where, Δt is the time step (unit: minute).

Experimental Design and Model Validation with a Greenhouse

Overview of the Experimental Greenhouse

The experimental greenhouse was a morel mushroom farm in Hanzhong City, Shaanxi Province (Figure 2). One greenhouse was selected within the farm, and the growth environment of morels in the greenhouse was used for data collection. The main structure of the greenhouse comprised a steel frame that was covered with plastic film, forming an overall arched shape. The greenhouse is 50 m long, 8 m wide, and the highest point of the arch is 2 m from the ground.

Figure 2. Images of the Morel Greenhouse Used in this Study

Experimental Design

The environmental variable acquisition systems used in greenhouse sheds primarily comprised soil sensors and air quality sensors that enabled the collection, transmission, and storage of data like soil temperature within 50 cm of the root system during the growth of Morchella, in addition to air temperature, humidity, and light intensity inside the shed, alongside atmospheric temperature and humidity outside the shed.

Soil temperature was measured with an FT-W485 temperature sensor that has a measurement accuracy of ± 0.5°C, an operating environment of −40°C to 85°C, and a measurement range of −40 to 80°C. The temperature sensors were placed in the experimental area of the greenhouse and buried at depths of 0.05, 0.15, 0.20, and 0.25 m from the surface (Figures 3 and 4).

Figure 3. Image of the Experimental Area Inside the Greenhouse Investigated in This Study

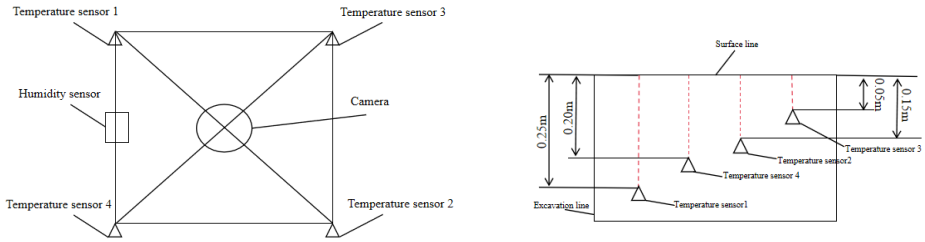

Figure 4. Schematic Showing Soil Temperature Sensor Positions

Air temperature and humidity were measured using a TVOC air quality sensor that has an operating temperature of 0–50°C and a working humidity range of 20–90% RH. One air quality sensor was placed inside the greenhouse, and another was placed outside. Solar radiation data were obtained by real-time monitoring from a weather station. The data collection intervals for the measurements were set to once per minute and included soil temperature and humidity inside the greenhouse, in addition to air temperature and humidity inside and outside the greenhouse. Data were collected from January to March 2024, while test data were collected on March 21, which was a sunny day. The primary reason for this is that the initial verification emphasized a sunny scenario characterized by stable solar radiation and minimal interfering factors, aiming to assess the rationality of the model mechanism. However, this limitation in the verification scenario may result in reduced prediction accuracy of the model under conditions of weak radiation and high humidity, such as during rainy days. Therefore, further validation using data from diverse weather conditions is essential in subsequent research. Other model input values are shown in Table 1.

Table 1. Parameter Values Used in the Modeling of Greenhouse Relative Humidity

Parameter	Value	Parameter	Value
Surface area of greenhouse covering material A	770 m^2	Solar radiation absorptivity α	0.92
Reflectivity of the plastic film rcs [18]	0.2	Convective heat transfer coefficient hc [21]	2.8 W/(°Cm2)
Emissivity of the plastic film Ɛ2 [19]	0.53	Psychrometric constant [22]	0.066 kPa/K
Thermal conductivity [20]	0.48 W/(mK)	Indoor air volume, Vair	1,200 m3
Thermal diffusivity of soil a [20]	7.06×10-7 m2/s	Soil evaporation coefficient ksoil	0.1 g/(h%)
Thermal radiation emissivity	0.92	Stefan-Boltzmann constant	5.67×10-8 W/(m-2K-4)

Model Evaluation

The Mean Bias Error (MBE) and Relative root mean square (rRMSE) performance statistical indicators are the most commonly employed metrics. MBE measures the overestimation or underestimation trends of models, while rRMSE values can indicate the degree of discrepancy between predicted and measured values. A negative MBE indicates overestimation, while a positive MBE indicates underestimation, wherein lower rRMSE values indicate higher model accuracy. These metrics are defined by Equations (19a) and (19b):

$$MBE = \frac{\Sigma(y_1 - y_2)}{n} \tag{19a}$$

$$rRMSE = \frac{100}{\bar{y}}\left(\sqrt{\frac{\Sigma(y_1 - y_2)^2}{n}}\right) \quad (19b)$$

where $\bar{y}$ is the mean of the measured data, y_1 is the measured data, y_2 is the calculated data, and n is the number of data points.

Results

Soil Temperature Predictions

Variation curves were constructed for outdoor air temperature, indoor air temperature (where both outdoor and indoor temperatures are measured and serve as input parameters in the model), and outdoor solar radiation on March 21, 2024 (at a sampling interval of 1 hour) (Figure 5). Outdoor temperature strongly correlated with solar radiation, increasing as solar radiation intensified and decreasing as it weakened. Indoor temperatures also rose due to solar radiation, with heating trends lagging compared to outdoor temperatures. Specifically, indoor temperatures will rise for some time after solar radiation peaks, because greenhouses exhibit heat preservation and storage capacity that can store solar radiation heat and slowly release it. Fluctuations in the range of indoor temperatures were relatively smaller than for outdoor temperatures, indicating that greenhouses buffer and regulate temperature, consequently reducing the interior impacts of drastic changes in external environmental temperatures.

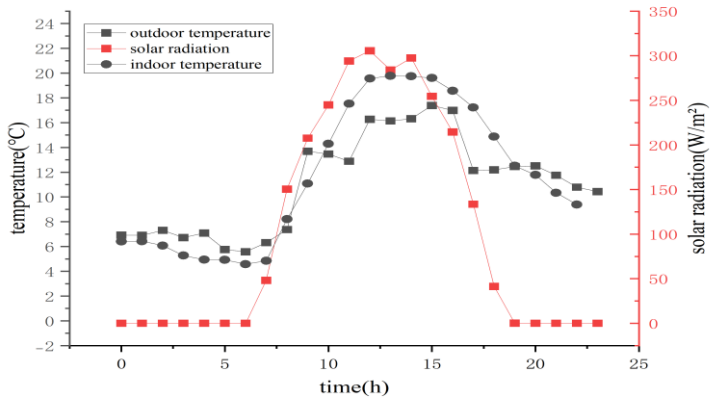

Figure 5. Hourly Variation of Temperatures Inside and Outside the Greenhouse in Addition to Solar Radiation

The variations in soil temperature within the greenhouse were measured at depths of 0.05 meters, 0.15 meters, 0.20 meters, and 0.25 meters (Figure 6). Soil temperatures at each depth generally first increased and then decreased over a day. As solar radiation intensifies and air temperature rises during the day, soils begin to absorb heat and warm. Then, when solar radiation dissipates at night and air temperature drops, soils release heat outward and cool. Soil temperature at a depth of 0.05 m exhibited the largest variation, with maximum temperature differences being 3.5°C. Soil temperature at a depth of 0.25 m

exhibited the smallest variation, with maximum temperature differences only being 0.5°C. The average soil temperatures at each depth (in the order of shallow to deep sections) were 12.8, 12.0, 11.9, and 11.7°C. Thus, soil temperature increases attenuated with increased soil depth, and the amplitude of soil temperature decreased.

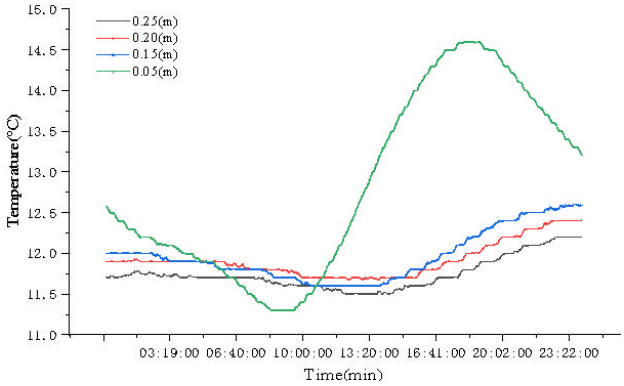

Figure 6. Hourly Variation of Greenhouse Soil Temperatures Measured at Depths of 0.05, 0.15, 0.2, and 0.25 m

Model-predicted temperatures at depths of 0.05, 0.15, 0.2, and 0.25 m were obtained by inputting the air temperature measurements inside and outside the greenhouse, in addition to solar radiation parameters, into Formula (13), followed by calculation over a 24-hour cycle at a sampling interval of 1 minute (Figure 7). The average predicted soil temperatures at depths of 0.05, 0.15, 0.2, and 0.25 m were 12.5, 12.2, 12.1, and 12.0°C respectively; the minimum soil temperatures were 9.35, 10.68, 11.14, and 11.47°C, respectively; while the maximum temperatures were 15.65, 13.61, 13.18, and 12.88°C, respectively. The minimum temperature increased with increased depth, while the maximum temperature decreased with increased depth. These results were similar to measured datasets, wherein soil temperature increases attenuated with increased soil depth, while the amplitude of soil temperature decreased.

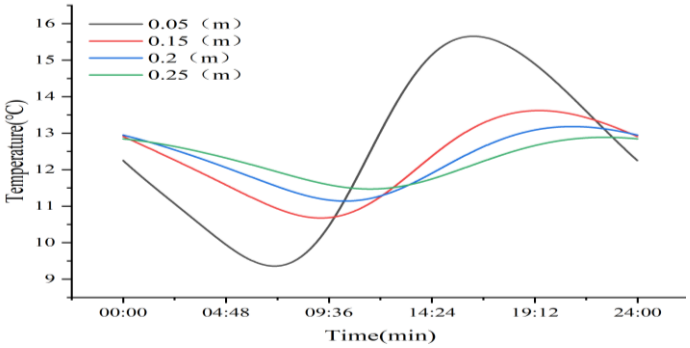

Figure 7. Simulated Greenhouse Soil Temperature Variation at Depths of 0.05, 0.15, 0.2, and 0.25 m

Comparisons of measured and predicted greenhouse soil temperatures were conducted at depths of 0.05, 0.15, 0.2, and 0.25 m (Figure 8). The degree of coincidence between the predicted and measured temperatures gradually increased with increased soil depth. At 0.05 m depth, the deviation between the predicted and measured values was relatively large, and especially during periods of drastic temperature changes, when visible differences were measured. However, the predicted values were closer to the measured values at depths of 0.15, 0.2, and 0.25 m, with highly similar values observed at 0.25 m depth.

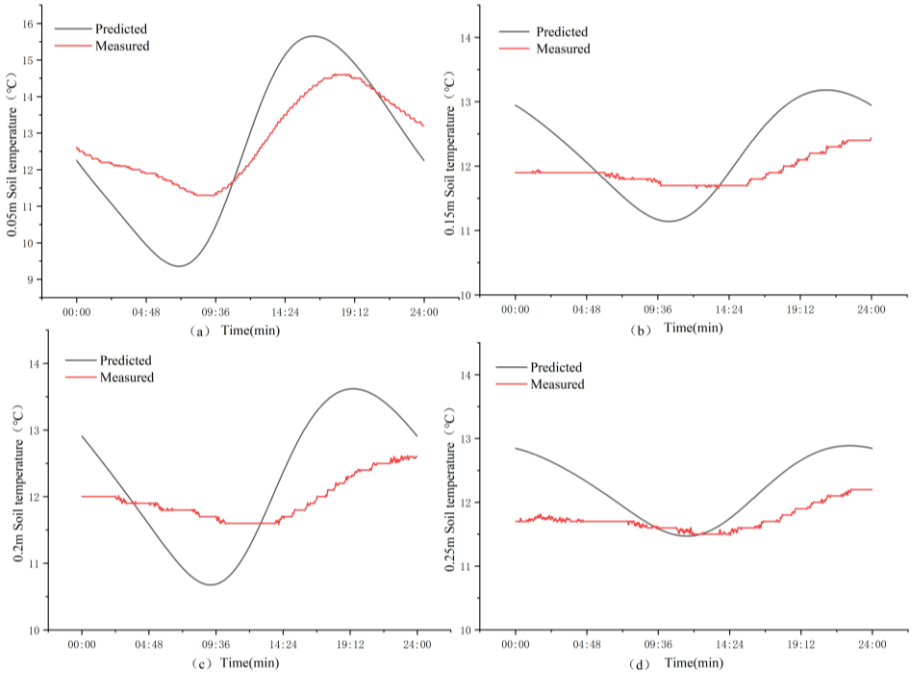

Figure 8. Comparison of Measured and Predicted Greenhouse Soil Temperature Values at Depths of 0.05, 0.15, 0.2, and 0.25 m

The statistical errors for predicted soil temperatures were calculated based on Formula (19) (Table 2). The maximum temperature differences between the measured and predicted values at depths of 0.05, 0.15, 0.2, and 0.25 m were 2.3, 1.4, 1.0, and 1.1°C, respectively. The MBE values at each depth were 0.29, −0.27, −0.32, and −0.49, while the rRMSE values at each depth were 10, 7, 5, and 5%, respectively. The analysis of the mean bias error (MBE) and relative root mean square error (rRMSE) values indicates that, compared to the mechanistic model proposed by Deng et al. [4] for predicting greenhouse soil temperature, this dynamic pseudo-mechanistic model demonstrates a superior ability to accurately simulate the dynamic fluctuations in indoor soil temperature. Nevertheless, certain discrepancies remain evident. These errors can be attributed to inherent accuracy issues associated with the measuring instruments themselves, which may also experience disturbances during installation and operation. Such factors contribute to deviations in the measured data, thereby reflecting inaccuracies when compared with predicted values. Additionally, environmental conditions within the greenhouse—such as light

intensity, ambient temperature, and humidity—exhibit continuous variations throughout the day. These fluctuations influence both surface temperature and water evaporation from the soil, further impacting its physical properties and leading to discrepancies between observed and predicted values. Moreover, it is important to note that physical and chemical characteristics of soil—including texture, porosity, and moisture content—vary at different depths. The aeration capacity and water conductivity of deeper soils differ significantly from those at the surface level; these distinctions affect various processes occurring within the soil matrix. Consequently, such complexities hinder accurate predictions by the model regarding actual conditions at varying depths, resulting in additional errors.

Table 2. Predicted Soil Temperature Errors

Error Type	0.05 m	0.15 m	0.20 m	0.25 m
Maximum Value Error	2.3	1.4	1.0	1.1
Mean Bias Error (MBE)	0.29	-0.27	-0.32	-0.49
Relative Mean Square Error (RMSE)	10%	7%	5%	5%

Analysis of Error Decomposition in Surface Soil

Figure 9 shows the time series of the error between the measured and predicted values at 0.05m. It can be observed from Figure 9 that the daily variation characteristics of the error are pronounced. During the daytime period (approximately 06:00 - 18:00), there is a significant increase in error, typically ranging from 0.2 to 0.8℃. In contrast, during the nighttime period, the error remains relatively small, predominantly within the range of 0.1 to 0.3℃. The maximum error occurs around 12:30, reaching up to 0.8℃, which aligns closely with the time of peak solar radiation. Furthermore, during the warming stage, the model tends to underestimate soil temperature (measured > predicted). Throughout this phase, while errors remain relatively minor, their direction appears uncertain.

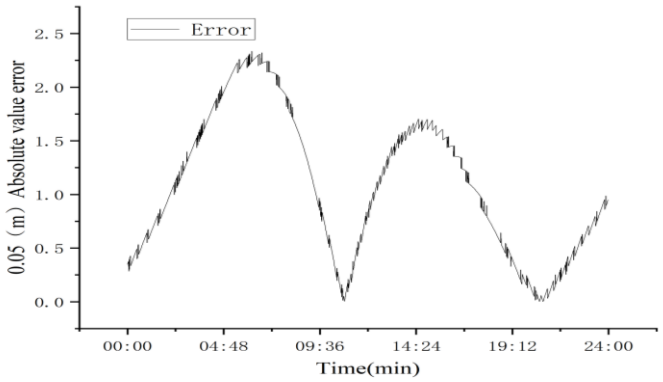

Figure 9. The Time Series of the Error between the Measured and Predicted Values at 0.05m

To quantify the primary sources of prediction errors in surface soil temperature, we conducted a correlation analysis utilizing high-frequency measured data. The Pearson correlation coefficient between the absolute error of soil temperature predictions at a depth of 0.05 meters and solar radiation intensity was calculated to be r =0.85 (n = 1437), indicating a strong positive correlation between the prediction error and solar radiation. This finding confirms that the dynamic surface effect—particularly the heat processes driven by solar radiation—is the predominant factor contributing to errors in predicting surface soil temperature. Further analysis revealed that these errors significantly increased during daytime hours with intense solar radiation (06:00 - 18:00), exhibiting an average absolute error of 0.42℃, whereas nighttime errors were only 0.18℃ on average. This pattern suggests that the model may underestimate the heating effects of solar radiation during daylight or overestimate evaporative cooling effects. Future optimizations of this model should prioritize integrating surface soil moisture sensors to dynamically calibrate evaporation terms, thereby enhancing prediction accuracy.

$$r = \frac{\sum_{i=1}^{n}\left(X_i - \overline{X}\right)\left(Y_i - \overline{Y}\right)}{\sqrt{\sum_{i=1}^{n}\left(X_i - \overline{X}\right)^2}\sqrt{\sum_{i=1}^{n}\left(Y_i - \overline{Y}\right)^2}} \quad (20)$$

In the formula, *Xi* represents the absolute error, *Yi* represents the solar radiation intensity, *X* and *Y* are the average values of the absolute error and solar radiation intensity respectively, and n = 1437.

Humidity Predictions

Greenhouse humidity was predicted over a 24-hour cycle at a sampling interval of 1 minute by inputting data for air temperatures inside and outside the greenhouse, air humidity outside the greenhouse, and solar radiation into Formula (14) (Figure 10). Variation in model-predicted values were basically consistent with measured values at most periods, although the overall predicted values were lower than the measured values. Air water vapor carrying capacity is weak during early morning to dawn, when temperature and light intensity are low. Thus, soil water evaporation is minimal at this time, and water vapor tends to easily condense, leading to relatively high humidity. As light intensity and temperature gradually increase, the air's capacity to hold water vapor increases, while soil water evaporation gradually weakens, causing humidity inside the greenhouse to decrease. In the afternoon, the temperature begins to decrease and light intensity gradually decreases, leading to slow declines in humidity. At night, the temperature further decreases, and insufficient light leads to increased water vapor condensation, leading again to increased humidity.

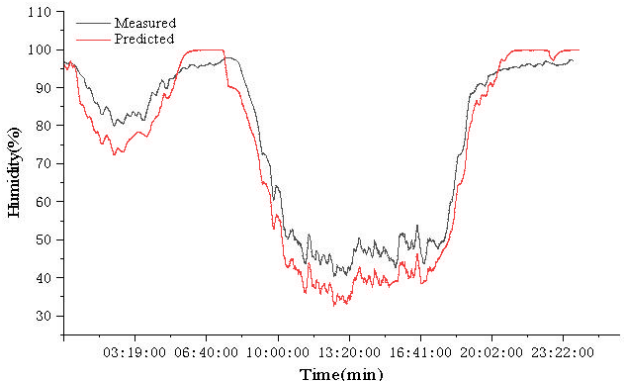

Figure 10. Comparison of Measured and Predicted Greenhouse Air Humidity Levels

Table 3. Predicted Air Humidity Error Statistical Metrics

Error Types	Relative Humidity
Maximum Absolute Error,%	8%
Mean Bias Error (MBE),℃:	4.027
Relative Root Mean Square Error (rRMSE),%	8.093%

The statistical errors for predicted air humidity were calculated using Formula (19) (Table 3). During the majority of the simulation period, the error in simulating relative humidity remained within 10%. This value is lower than the relative mean square error of 8.6% reported for indoor humidity in a rose greenhouse in Zimbabwe, as simulated by Mashonjowa et al. [23] using the GDGCM dynamic mechanism model. These findings indicate that this dynamic pseudo-mechanism model is capable of accurately capturing the dynamic variations in indoor humidity.

The humidity model (Equation 14) presented in this study solely accounts for the effects of soil evaporation and ventilation on air humidity, neglecting the contribution of biological water sources released during the growth of Morchella. This omission is a critical factor contributing to the underestimation of humidity within the model system (MBE = +4.027). As a fungal organism, Morchella exhibits notable water release characteristics: (1) Water production from mycelial metabolism: Upon absorbing soil moisture, mycelium generates water through biosynthetic reactions, yielding approximately 0.6 g of water per gram of dry matter synthesized; (2) Water release from transpiration of fruiting bodies: The transpiration occurring on the surface of fruiting bodies is influenced by variations in air humidity. Field measurements indicate that during sunny afternoons in March, each square meter of Morchella fruiting bodies can release between 0.08 and 0.10 g of water per hour.This biological source of water directly enhances air humidity within greenhouse environments but was not incorporated into the original model framework. Consequently, this led to an underestimation in total calculated water input compared to actual values, ultimately resulting in predicted humidity levels being lower than those measured experimentally.

Discussion

In this study, a greenhouse soil temperature model that considers heat transfer processes, such as convection, thermal conduction, radiation, and water evaporation, is developed. The model predicts soil temperature based on inputs of solar radiation and indoor/outdoor air temperatures. An indoor greenhouse air humidity model is then constructed that considers water vapor substance changes (e.g., via soil evaporation, ventilation, and humidification) and the law of mass conservation. The model thus predicts indoor air humidity based on data inputs of indoor air temperature, outdoor air temperature, and outdoor air humidity. Both models are validated using experimental greenhouse measurements.

The soil temperature prediction model constructed based on the one-dimensional heat transfer assumption adequately captures daily variation in soil temperatures at different depths. The overall consistency between the measured and predicted values significantly improves with increasing soil depth. Specifically, the relative root Mean Square Error (rRMSE) at a depth of 0.25 m is 5%, indicating that the model accurately depicts heat transfer processes in deep soils. At a depth of 0.05 m, the soil surface layer is strongly affected by dynamic factors such as solar radiation and water evaporation, with a relative root Mean Square Error (rRMSE) of 10%, indicating greater deviations in predictions.

Soil temperatures exhibit intense fluctuations in the shallow layer and stability in the deep layer, with the maximum temperature difference at 0.05 m reaching 3.5°C, but only 0.5°C at 0.25 m. Additionally, the average temperature gradually decreases with increasing depth (from 12.5°C to 12.0°C), confirming the attenuation of soil heat conduction. The trend predicted by the model, wherein maximum temperature decreases with depth and the minimum temperature increases with depth, is consistent with measured results, indicating that the model can reflect vertical differences in soil heat storage and heat dissipation.

The air humidity within the greenhouse is influenced by various factors, including light intensity, external humidity levels, and soil evaporation. Analysis of the measured data indicates that condensation is likely to occur during the early morning hours due to low temperatures and high humidity. In contrast, as temperatures rise in the afternoon, humidity levels decrease; however, they experience a slight increase at night owing to radiative cooling. While the current humidity model effectively captures trends in humidity fluctuations, it does not account for the biological water source associated with morel mushrooms (fungi), resulting in an overall predicted value that falls short of observed measurements. This discrepancy yields an average bias variance error of 4.027. Future research will concentrate on quantitatively modeling this biological water source. Through laboratory experiments and greenhouse monitoring efforts, we aim to establish a correlation model linking 'morel growth' with 'biological water release.' This model will subsequently be integrated into our humidity prediction formula to enhance its adaptability to the complex water sources present within greenhouses.

Quantitative analysis indicates a strong positive correlation between the prediction error of the 0.05-meter surface soil temperature and the intensity of solar radiation, with a Pearson correlation coefficient (r) of 0.85. This finding precisely suggests that the dynamic surface effect driven by solar radiation is the primary source of prediction errors at the surface level. Furthermore, it is observed that the error during

daytime (average 0.42℃) significantly exceeds that observed at night (average 0.18℃). This discrepancy confirms the limitations of the model in accurately representing the intense energy exchange processes occurring between surface soil and atmosphere, particularly regarding the balance between radiative heating and evaporative cooling processes.

This study, based on a small-scale application in conventional greenhouse sheds, developed a temperature and humidity prediction model that effectively balances accuracy and cost-efficiency. However, there are two notable limitations: first, the validation of the model was restricted to sunny conditions and did not comprehensively evaluate its robustness under cloudy or rainy scenarios; second, the humidity model failed to account for biological water sources, while the soil temperature model did not fully achieve dynamic parameter adjustment. Future research should focus on enhancing experimental verification across diverse weather conditions, improving the quantification of biological water sources, and optimizing dynamic parameters. This will provide more comprehensive technical support for the low-cost intelligent transformation of greenhouse sheds and facilitate the widespread adoption of precise environmental control in facility agriculture.

Funding

Shaanxi Provincial Science and Technology Plan Development Project 2025QCY-KXJ-015.

Shaanxi Provincial Science and Technology Plan Development Project 2025CY-YBXM-378.

References

[1] Huang Tao. (2020). *Research on Integration of Biomass Heating System for Greenhouses in Hot Summer and Cold Winter Climate Zone*. Hunan University.

[2] Ministry of Agriculture and Rural Affairs, National Development and Reform Commission, Ministry of Finance, & Ministry of Natural Resources. (2023). Notice on issuing the National Plan for the Construction of Modern Facility Agriculture (2023-2030). *Bulletin of the Ministry of Agriculture and Rural Affairs of the People's Republic of China*, (8), 6-33.

[3] Sun, Y. B., Gao, L. A., Jia, Y. C., et al. (2025). Construction and validation of a dynamic simulation model for temperature and humidity in northern photovoltaic solar greenhouses. *Journal of Shandong Agricultural University* (Natural Science Edition), *56*(1), 58-73.

[4] Lianhua, D., Lin, H., Ying, Z., et al. (2023). Analytic model for calculation of soil temperature and heat balance of bare soil surface in solar greenhouse. *Solar Energy*, *2023*, 249312-326.

[5] Chen, J. X., & Du, Z. Y. (2024). Construction of an indoor temperature and humidity prediction model for solar greenhouses based on bare soil surfaces. *Acta Energiae Solaris Sinica*, *45*(8), 414-422.

[6] Pan, J. G., Liu, P. Z., Zhang, Y., et al. (2024). Study on a temperature and humidity prediction model for solar greenhouses based on SSA-Elman. *Journal of Chinese Agricultural Mechanization*, *45*(11), 69-76.

[7] Feng, D. G., Feng, S. Z., Li, Z. X., et al. (2025). Comparison of temperature prediction methods for

solar greenhouses based on multiple linear regression models. *Journal of Shenyang Normal University* (Natural Science Edition), *43*(1), 75-81.

[8] Dewi, K. A. V., Setiawan, I. B., Minasny, B., et al. (2020). Modeling air temperature inside an organic vegetable greenhouse. *Agrivita Journal of Agricultural Science*, *42*(2), 295-305. https://doi.org/10.17503/agrivita.v0i0.2526

[9] Kim, J., & You, F. (2025). Energy-efficient greenhouse climate control using Gaussian process-based stochastic model predictive control. *Applied Energy*, *2025*, 391125841-125841. https://doi.org/10.1016/j.apenergy.2025.125841

[10] Xiong, Y., & Su, Y. (2025). Hybrid modeling approaches for accurate greenhouse climate prediction: Combining mechanistic models and LSTM neural networks. *Ecological Modelling*, *2025*, 503111059-111059. https://doi.org/10.1016/j.ecolmodel.2025.111059

[11] Mahmood, F., Govindan, R., & Ansari, A. T. (2025). Efficient energy management and temperature control of a high-tech greenhouse using an improved data-driven model predictive control. *Energy Conversion and Management: X*, *2025*, 26100939-100939. https://doi.org/10.1016/j.ecmx.2025.100939

[12] Mallick, S., Airaldi, F., Dabiri, A., et al. (2025). Reinforcement learning-based model predictive control for greenhouse climate control. *Smart Agricultural Technology*, *2025*, 10100751-100751. https://doi.org/10.1016/j.atech.2024.100751

[13] Bernardo, M., Wenjie, Y., Sjoerd, B., et al. (2023). Reinforcement Learning versus Model Predictive Control on greenhouse climate control. *Computers and Electronics in Agriculture*, *2023*, 215. https://doi.org/10.1016/j.compag.2023.108372

[14] Oybek, E., & ChulHee, L. (2023). Performance Analysis of Time Series Deep Learning Models for Climate Prediction in Indoor Hydroponic Greenhouses at Different Time Intervals. *Plants* (Basel, Switzerland), *2023*, *12*(12). https://doi.org/10.3390/plants12122316

[15] Akshay, A., S. N. M., & Fengqi, Y. (2023). Energy-efficient AI-based Control of Semi-closed Greenhouses Leveraging Robust Optimization in Deep Reinforcement Learning. *Advances in Applied Energy*, *2023*, 9. https://doi.org/10.1016/j.adapen.2022.100119

[16] Zhang, X. (2014). *Heat transfer* (6th ed.). China Architecture & Building Press. (in Chinese)

[17] Tiwari, G. (2003). *Greenhouse Technology for Controlled Environment*.

[18] Deng, W., Luo, J., & Li, X. (2013). Simulation of temperature and humidity in plastic greenhouses under natural ventilation conditions. *Journal of Irrigation and Drainage*, *32*(02), 10-14.

[19] Ma, C. (2005). *Agricultural bioenvironmental Engineering*. China Agriculture Press. (in Chinese)

[20] Papadakis, G., Frangoudakis, A., & Kyritsis, S. (1989). Soil energy balance analysis of a solar greenhouse. *Journal of Agricultural Engineering Research*, *43*, 231-243. https://doi.org/10.1016/S0021-8634(89)80021-6

[21] Sethi, V. P. (2009). On the selection of shape and orientation of a greenhouse: Thermal modeling and experimental validation. *Solar Energy*, *83*(1), 21-38.

https://doi.org/10.1016/j.solener.2008.05.018

[22] Min Qian. (2001). Predicting Water Surface Evaporation by Using Penman Formula. *Advances in Science and Technology of Water Resources*, *21*(1), 37-39.

[23] Mashonjowa, E., Ronsse, F., Milford, J., et al. (2013). Modelling the thermal performance of a naturally ventilated greenhouse in Zimbabwe using a dynamic greenhouse climate model. *Solar Energy*, *2013*, 91381-393. https://doi.org/10.1016/j.solener.2012.09.010